

INITIAL EEX-BASED BUNCH SHAPING EXPERIMENTAL RESULTS AT THE ARGONNE WAKEFIELD ACCELERATOR FACILITY

Gwanghui Ha, Moohyun Cho, and Won Namkung,
 POSTECH, Pohang, Gyeongbuk 790-784, KOREA

Manoel Conde, Darrell Scott Doran, Wei Gai, Kwang-Je Kim, Wanming Liu, John Gorham Power,
 Yin-E Sun, Charles Whiteford, Eric Edson Wisniewski, and Alexander Zholents

Argonne National Laboratory, Argonne, IL 60439, USA

Chunguang Jing, Euclid TechLabs, Solon, Ohio 44139, USA

Philippe Regis-Guy Piot, Fermi National Accelerator Laboratory, Batavia, IL 60510, USA

Abstract

A program is under development at Argonne National Laboratory to use an emittance exchange (EEX) beamline to perform longitudinal bunch shaping (LBS). The double dog-leg EEX beamline was recently installed at the Argonne Wakefield Accelerator (AWA) and the goals of the proof-of-principle experiment are to demonstrate LBS and characterize its deformations from the ideal shape due to higher-order and collective effects. The LBS beamline at the AWA consists of insert-able transverse masks mounted on an actuator and four quadrupoles (to manipulate the transverse phase space) before the EEX beamline, which consists of two identical dog-legs and a deflecting cavity. The mask and input beam parameters are varied during the experiment to explore the shaping capability and clarify the deformation sources and their mitigation. Progress on the commissioning of the LBS beamline, initial experimental data and benchmarks to GPT [1] simulations will be presented.

EMITTANCE EXCHANGE BEAMLINE AT ARGONNE WAKEFIELD ACCELERATOR FACILITY

The emittance exchange (EEX) is an attractive tool to manipulate the phase space because of its unique characteristics [2]. In the EEX beam line, the entire longitudinal beam properties at the downstream are governed only by the upstream transverse properties. This characteristic can be applied to generate an arbitrary current profile for many applications [3]. The Argonne Wakefield Accelerator (AWA) is planning to demonstrate longitudinal bunch shaping (LBS) using EEX [4,5]. The EEX beam line was installed at the downstream of the AWA drive beam line last year and experiments have started this year. The EEX experiment at the AWA will take place in three stages: (1) EEX demonstration, (2) LBS demonstration, and (3) deformation study. Recently, we successfully finished the stage (1) and we present the experiment results here.

There are several different varieties of EEX beam lines [2,6,7], and the AWA installed the double dog-leg EEX beam line for the initial study. This beam line consists of four rectangular dipole magnets which make two identical

dog-legs and one transverse deflecting cavity (TDC) as shown in Fig. 1. The linear transport matrix for the beam coordinate $X = [x, x', z, \delta]$ with $1 + \kappa\eta = 0$ condition is

$$R = \begin{bmatrix} 0 & L_c/3 & \kappa L_s & \eta + \kappa\xi L_s \\ 0 & 0 & \kappa & \kappa\xi \\ \kappa\xi & \eta + \kappa\xi L_s & L_c\kappa^2\xi/6 & L_c^2\kappa^2\xi^2/6 \\ \kappa & \kappa\xi L_s & L_c\kappa^2/6 & L_c\kappa^2\xi/6 \end{bmatrix}, \quad (1)$$

where L_s is $L + L_{bc} + L_c/3$, L is $(2L_b \cos \alpha + L_{bb})/\cos^2 \alpha$, η is $(2L_b \cos^2 \alpha - 2L_b \cos \alpha - L_{bb} \sin^2 \alpha)/(\sin \alpha \cos^2 \alpha)$, ξ is $(L_{bb} \sin^3 \alpha + 2L_b \sin \alpha - 2\alpha L_b \cos^2 \alpha)/(\sin \alpha \cos^2 \alpha)$, α is the bending angle, L_b is the length of the dipole magnet, L_{bb} is the distance between dipoles, L_{bc} is the distance between the dipole and the TDC. L_c is the length of the TDC, and $\kappa (= \frac{eV 2\pi}{E \lambda})$ is the deflecting cavity kick strength [4,8].

The beam line parameters (Table 1) were chosen to simultaneously insure compatibility with the existing AWA facility and satisfy EEX requirements. The dispersion created by the dog-leg was large enough for the TDC [8]. The charge of the bunch at the entrance of the exchanger was set to 5 nC such that the charge after Table 1: Beam Line and Input Beam Parameters used in the EEX Experiment

Beam line parameters	Value	Unit
Bending angle	20	deg
Dipole-to-Dipole distance	2.0	m
Dipole-to-TDC distance	0.5	m
η (dispersion of dog-leg)	0.9	m
ξ (momentum compaction of dog-leg)	0.3	m
κ (TDC kick strength)	-1.1	m ⁻¹
Input beam parameters	Value	Unit
Beam energy	46.5	MeV
Charge before mask	5	nC
Charge after mask	~1	nC
Beam size at EY1	5	mm
Transverse emittance	25	μm
Bunch length	1	mm
Energy spread	0.5	%

#homehe@postech.ac.kr

Content from this work may be used under the terms of the CC BY 3.0 licence (© 2015). Any distribution of this work must maintain attribution to the author(s), title of the work, publisher, and DOI.

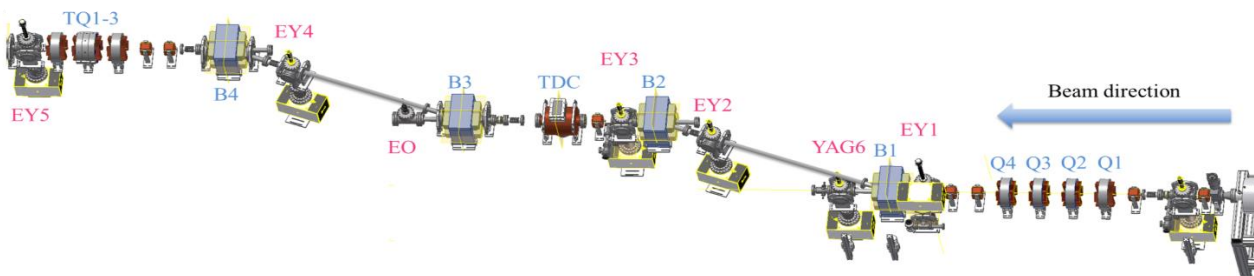


Figure 1: EEX beam line configuration at the AWA. EY, EO and YAG show the YAG screen positions. Q and TQ are the quadrupole magnets. B is the dipole magnets. TDC is the transverse deflecting cavity.

the mask is more than 1 nC. The initial laser pulse length is set to 8 ps FWHM and linac phases are set to achieve maximum energy gain. The beam size at EY1 was chosen to be 5 mm, first to achieve long enough bunch length at the end of EEX beam line to be compatible with the diagnostic resolutions, and second since a large beam size and mask reduces the sensitivity to the beam position error.

The dispersion of the first dog-leg was checked from the transverse offset measurement at position EO by varying the magnetic field strength. Since the magnet is not located on the ideal position, measured dispersion of 0.86 m was deviated from the calculated dispersion of 0.89 m (magnet position will be corrected in the stage (2) and (3)). The TDC was also calibrated and the power was chosen based on the $1 + \kappa\eta = 0$ condition.

The masks described in Ref [5] will be used for all three stages of the experiment, and we tested two of them during stage (1). The two-slit mask and the fish-shaped mask were used for the stage (1) experiment to generate two transverse beamlets. The transverse densities of the beam at the downstream of each masks measured at YAG6 are displayed in Fig. 2. The corresponding peak current distribution have two flat-top shapes and the triangle shape.

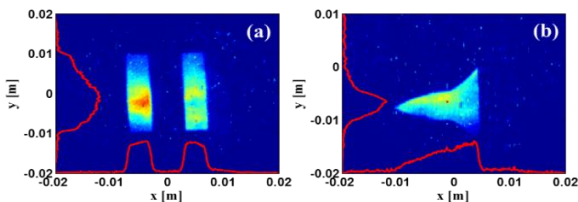


Figure 2: Transverse beam images at YAG6 taken with the two-slit mask (a) and the fish-shaped mask (b) to generate the longitudinal two bunch train and the triangle profile respectively.

SIMULATION FOR STAGE 1 EXPERIMENT

Simulation was carried out before the stage (1) experiment to guide the experiment. The General Particle Tracer (GPT) was used with its own 3D space-charge routine [1]. Since CSR was a significant effect during the experiment, CSR routine was implemented in GPT. This CSR routine was developed and benchmarked by I. V.

Bazarov [9] and we also benchmarked this routine with Elegant and CSRTrack.

In Fig. 3, GPT simulation and experiment results are seen to be in a reasonable agreement. The right column of Fig. 3 shows simulated transverse beam images at each YAG screen positions and the left column shows corresponding images taken during the experiment. The first row shows the round beam with a rms size of ~ 5 mm. At position EO, the beam is wide due to the vertical focusing from the dipole edges and the dispersion in the horizontal plane as can be seen in the second row of Fig. 3. The third row of Fig. 3 is the image at EO position with the two-slit mask. Although the first dog-leg and deflecting cavity provide a partial exchange, it is only for the transverse and longitudinal momentums. Thus, the initial horizontal position properties still affect the transverse images at the EO position as implied by Eq. (2) which is the transport matrix up to EO position.

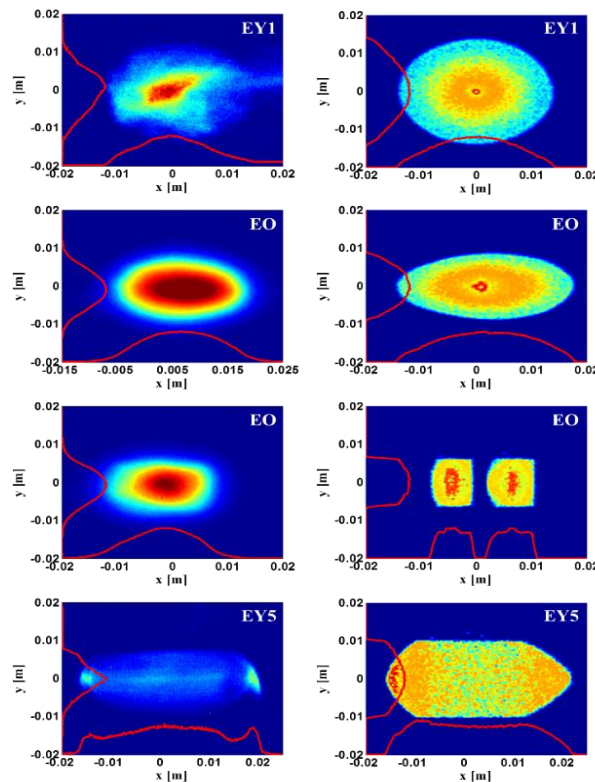


Figure 3: Transverse beam images at each YAG positions. Left and right columns respectively correspond to the experiment and the simulation result.

$$R = \begin{bmatrix} 1 & L_1 & \kappa L_2 & \eta + \kappa \xi L_2 \\ 0 & 0 & \kappa & \kappa \xi \\ 0 & \eta & 1 & \xi \\ \kappa & \kappa L_s & L_c \kappa^2 / 6 & L_c \kappa^2 \xi / 6 \end{bmatrix}, \quad (2)$$

where L_1 is $L + L_{bc} + L_c/2$ and L_2 is $L_{bc} + L_c/2$. When the two-slit mask is applied to the beam, the image at position EO consists of two beamlets; see third row of Fig. 3. The beamlets are not seen in the experimental image because the YAG screen was placed in the air side behind a quartz vacuum window which lead to a significant multiple scattering (the setup will be improved for stage (2) and (3)). At EY5, the beam has an interesting horizontal feature because the horizontal properties at this position are due to the longitudinal properties at the entrance to the exchanger. Both simulated and experimented beam show a round edge on the left side and a sharper edge on the right side. Because of the two-slit mask, the top and bottom of image have a knife-edge.

EVIDENCE OF EEX

To demonstrate EEX, it is possible to measure both the transverse and longitudinal emittances before and after the EEX beam line [10]. However, we concentrated on exploring the key features of the EEX beam line. If the EEX is working correctly, then two beams that are separated longitudinally should become two transversely separated beams. Similarly, two beams that are transversely separated should be converted to two longitudinally separated beams [11]. Since we could measure the transverse properties only, the two-slit mask was applied at the entrance to the exchanger to generate two transversely separated beams. The last row in Fig. 3 shows the transverse beam image at EY5 position and this image shows a single beam. In the middle of the beam, particles are almost uniformly distributed and each end has a higher density. This distribution matches well with the GPT simulations of the transverse image at EY5 and the initial longitudinal distribution after the mask.

If EEX is not working properly, each beam would be spread out by the dispersion and they would appear as a single beam because of overlap. In this case, the transverse image at EY5 should show a weakly modulated large beam. However, it may hard to see this weak modulation on the YAG screen. To make sure that EEX is working, we tested this feature in another way.

A quadrupole magnet always focuses the beam in one direction while defocusing the beam in the other direction. In the EEX beam line, however, the downstream horizontal profile only depends on the upstream longitudinal profile. Therefore, if a quadrupole is used to focus/defocus the beam before the EEX, only the vertical beam size at EY5 would change. During the experiment, Q1 varied from -0.7 T/m to 0.7 T/m. Fig. 4 shows the transverse beam images at EY5 with different Q1 strengths. While the vertical beam size changes dramatically, the horizontal beam size remains approximately constant. The actual beam size was given

in Fig. 4 (d). The vertical beam size changes from 3 mm to 8 mm, and the horizontal beam size changes from 10 mm to less than 11 mm. There is small variation on the horizontal beam size. This change comes from the thick-lens effect given in Eq. (1) which is expected.

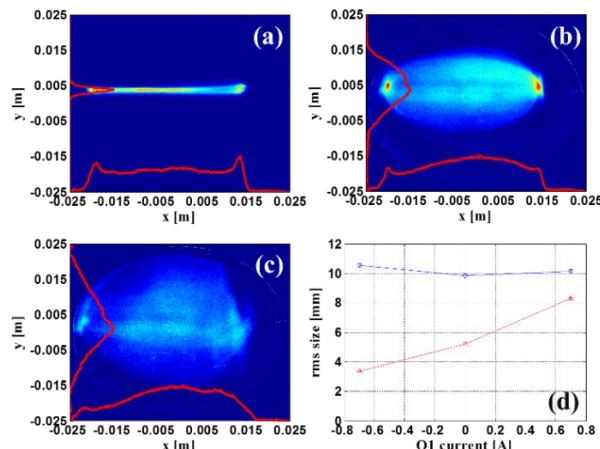


Figure 4: Transverse beam image at EY5 with Q1 current of -0.7 T/m (a), 0 T/m (b), and 0.7 T/m (c). Horizontal and vertical beam size at each current (d).

FUTURE WORK

Both Fig. 3 and Fig. 4 prove the EEX is working properly in the AWA EEX beam line. Also, the experimental observation of the beam images matches well with the linear matrix and GPT simulation results. Based on the results with the two-slit mask, we expect that LBS will work well. For the second and third stage, we will install the deflecting cavity for current profile measurements and vary the input beam condition to understand the sources of deformation and its mitigation. The installation and experiment will be completed this year.

REFERENCES

- [1] www.pulsar.nl/gpt
- [2] P. Emma et al., Phys. Rev. ST Accel. Beams **9**, 100702 (2006).
- [3] P. Piot et al., Phys. Rev. ST Accel. Beams **14**, 022801 (2011).
- [4] G. Ha et al., AIP Conf. Proc. **1507**, 693 (2012).
- [5] J. Power et al., Proceedings of IPAC 2014, Dresden, Germany, pp. 1506-1508 (2014).
- [6] D. Xiang and A. Chao, Phys. Rev. ST Accel. Beams **14**, 114001 (2011)
- [7] C. R. Prokop et al., Proceedings of IPAC 2013, Shanghai, China, pp. 3103-3105 (2013).
- [8] M. Conde et al., Proceedings of IPAC 2012, New Orleans, LA, USA, pp. 3350-3352 (2012).
- [9] I. V. Bazarov and T. Miyajima, Proceedings of EPAC 2008, Genoa, Italy, pp. 118-120 (2008).
- [10] T. W. Koeth et al., Proceedings of IPAC 2009, Vancouver, Canada, pp. 4350-4352 (2009).
- [11] Y.-E Sun et al., Phys. Rev. Lett. **105**, 234801 (2010).